Stochastic resonance in optical bistable systems

Roland Bartussek and Peter Hänggi
Department of Physics, University of Augsburg, Memminger Strasse 6, D-86135 Augsburg, Germany

Peter Jung
University of Illinois at Urbana-Champaign, Beckman Institute, 405 North Mathews Avenue, Urbana, Illinois 61801
(Received 7 December 1993)

We study the response of a noise-driven absorptive optical bistable system which is subjected to deterministic periodic perturbations of the incident light intensity. This system is characterized by state-dependent noise which in turn can strongly enhance—via stochastic resonance—the response due to the external periodic perturbation. We demonstrate that the condition for stochastic resonance sensitively depends on the shape of the bistable generalized potential (symmetric or asymmetric). Furthermore, the generation of higher harmonics is studied in the presence of fluctuations. We report on a novel phase-sensitive resonance phenomenon which virtually eliminates the higher harmonics and thus allows for distortion-free amplification of signals via stochastic resonance.

PACS number(s): 05.40.+j, 05.20.−y, 42.65.Pc

I. INTRODUCTION

The concept of stochastic resonance (for a collection of papers, see [1–7]) has been developed to explain the more or less periodic occurrences of ice ages. The basic idea is that the fluctuation induced transitions between a metastable high temperature and low temperature state of the global earth climate are synchronized by the weak periodic changes of the earth-orbit eccentricity, thereby yielding a strong enhancement of the climate's response. Theoretical investigations [1–5] have shown that the amplitude of the response of a noisy, bistable system to small periodic forcing actually shows a maximum approximately at that value of the noise strength, at which the period of the driving force matches twice the system's sojourn time in the (symmetric) stable states (a more refined transcendental equation for the position of the maximum has been derived recently in Ref. [4]). This noise-induced enhancement of the response has been termed stochastic resonance.

Further evidence of stochastic resonance has been found in an experiment on a shorter time scale, i.e., by studying the switching statistics of a bistable ring laser [2]. Here, the probabilistic weights of the clockwise and counterclockwise propagating laser modes are periodically modulated, yielding synchronization of the noise-induced hopping between the two modes. The quantity which has been studied in this experiment is the signal-to-noise ratio. It has been obtained by measuring the power spectrum of one of the modes. Such a power spectrum typically shows a Lorentzian-like background with an additional sharp peak at the driving frequency and additional (but much smaller) peaks at higher harmonics [3,5]. The signal-to-noise ratio, defined by the ratio of the weight of the peak at the driving frequency and the background power collected from a small bandwidth around this peak, exhibits a resonancelike peak as a function of the noise strength. Stochastic resonance has also been demonstrated in a periodically modulated noisy Schmitt trigger [6], and very recently also in periodically stimulated mechano-receptor cells of cray fishes [7].

In this paper we focus on the theory for stochastic resonance in *asymmetric* continuous systems which are driven by *state-dependent* (or multiplicative) noise [8]. As a working model we use the standard model for absorptive optical bistability. A weak, periodic modulation of the incident light amplitude yields a signal in the transmitted light amplitude at the fundamental external frequency, and higher harmonics as well. We take into account fluctuations in the inversion of the population in the atomic levels, yielding a noisy transmitted amplitude. The central problem we are addressing in this paper is the impact of noise on the transmission of the periodic modulation through the optical bistable system.

We remark, however, that our specific results for stochastic resonance in optical bistability have a broader validity, i.e., the novel characteristic features hold qualitatively true for other applications characterized by potential-asymmetry, periodic modulation, and additive or multiplicative fluctuations [9].

In Sec. II, we introduce the model and present a brief sketch of the theory. In Sec. III we discuss in detail the amplification of the periodic modulation of the incident light and compare our numerical results with the analytical findings obtained by using linear response theory. Also of interest is the generation of higher harmonics due to the nonlinearity of the system in the presence of noise. The amplitudes of the higher harmonics are studied as a function of the noise in Sec. IV. The amplitudes of some higher harmonics show a very peculiar phenomenon, namely *resonancelike suppression at certain values of the noise strength*—a phenomenon which has recently also been found in a two-state system [9]. These novel noise-induced resonances are—in contrast to stochastic resonance—phase sensitive, i.e., the phases of higher harmonics, discussed in Sec. V, exhibit at small

modulation frequencies well defined jumps, which are located precisely at those resonances. Our conclusions are given in Sec. VI. In the Appendix we describe the numerical technique we are using to obtain high-precision results.

II. MODEL AND BASIC EQUATIONS

A model for purely absorptive optical bistability in an optical cavity was introduced by Bonifacio and Lugiato [10]. For the amplitude y of the input light and the transmitted amplitude x they have derived the equation of motion for the dimensionfree variables as

$$\frac{dx}{dt} = y - x - \frac{2cx}{1+x^2} = -\frac{dV(x)}{dx}, \tag{2.1a}$$

where the potential $V(x)$ reads

$$V(x) = -\int^x \left(y - x' - \frac{2cx'}{1+x'^2}\right) dx'$$
$$= -yx + \frac{x^2}{2} + c\ln(1+x^2), \tag{2.1b}$$

and where the parameter c is proportional to the inversion of the population of the atomic levels. In Fig. 1, the stationary values of the transmitted amplitude x are shown as a function of the input light amplitude y for various values of the inversion c. At small values of the inversion, there is one stationary value of the transmitted amplitude for fixed y. For larger inversion, the input-output characteristics show bistability, i.e., there are three stationary transmitted amplitudes with the smallest and the largest ones being stable, and the intermediate being unstable. In terms of the potential $V(x)$, we find two minima of $V(x)$ when the system exhibits optical bistability (see Fig. 2).

Having chosen a value for the input intensity $y \equiv y_0$ within the regime of bistability, we next periodically modulate this value with the amplitude A, frequency Ω, and phase Ψ. In Eqs. (2.1) we then have to substitute the value y by

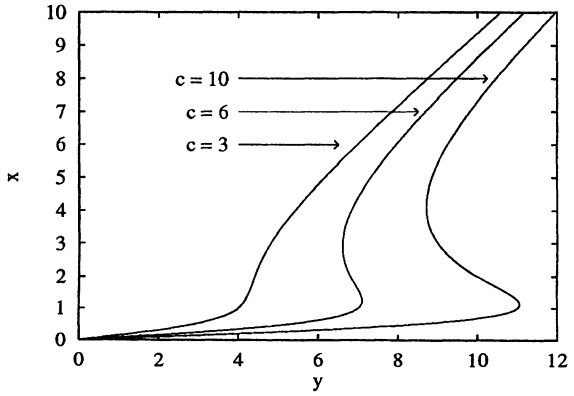

FIG. 1. The stationary states of the output light amplitude x of an optical bistable element are shown versus the input light amplitude y for various values of the parameter c.

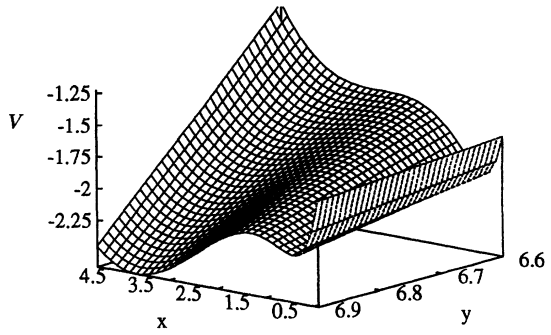

FIG. 2. The potential $V(x)$ (2.1) is plotted versus the input and output light amplitudes y and x.

$$y(t) = y_0 + A\cos(\Omega t + \Psi). \tag{2.2}$$

We also take into account fluctuations of the inversion c due to spontaneous emission processes, collisions of atoms, or fluctuations of the atomic density in the cavity [11]. We assume that these fluctuations are fast and can be modeled by white Gaussian noise $\Gamma(t)$ of vanishing mean, i.e. [11],

$$c \to c + \frac{\sqrt{D}}{2}\Gamma(t), \tag{2.3}$$

and noise correlation

$$\langle \Gamma(t)\Gamma(t')\rangle = 2\delta(t-t') \tag{2.4}$$

with D denoting the noise intensity. The time dependence of the transmitted light amplitude x is thus described by the nonlinear (Stratonovich) Langevin equation with multiplicative noise, i.e.,

$$\frac{dx}{dt} = y(t) - x - 2c\frac{x}{1+x^2} + \frac{x}{1+x^2}\sqrt{D}\Gamma(t), \tag{2.5}$$

being equivalent with a nonstationary Markovian stochastic process. The corresponding probability density $P(x,t;\Psi)$ of the transmitted light amplitude x obeys the Fokker-Planck equation

$$\frac{\partial}{\partial t}P(x,t;\Psi) = \left\{-\frac{\partial}{\partial x}\left[D^{(1)}(x) + A\cos(\Omega t + \Psi)\right] + \frac{\partial^2}{\partial x^2}D^{(2)}(x)\right\}P(x,t;\Psi), \tag{2.6a}$$

where the drift is given by

$$D^{(1)}(x) = y_0 - x - 2c\frac{x}{1+x^2} + D\frac{x(1-x^2)}{(1+x^2)^3}, \tag{2.6b}$$

and the state-dependent diffusion reads

$$D^{(2)}(x) = D\frac{x^2}{(1+x^2)^2}. \tag{2.6c}$$

In the absence of the modulation of the input light amplitude, i.e., $A = 0$, the probability density approaches for large times the stationary probability density

$$P_{st}(x) = Ng(x)\exp\left(-\frac{\Phi(x)}{D}\right), \tag{2.7}$$

where g is given by

$$g(x) = \frac{1+x^2}{x}, \tag{2.8a}$$

and where the noise-induced, generalized potential reads

$$\Phi(x) = \frac{y_0}{x} - 2xy_0 + x^2(1+c) - x^3\frac{y_0}{3} + \frac{x^4}{4} + (1+2c)\ln x. \tag{2.8b}$$

The quantity N denotes the (numerically determined) normalization constant. The stationary probability density shows two maxima if the parameters c and y_0 are chosen such that our system is bistable (Fig. 3).

In the *presence of modulation*, the probability density $P(x,t;\Psi)$ eventually approaches a periodic function $P_{as}(x,t;\Psi)$ in time, with the period given by the period of the modulation [12]. The asymptotic long-time response $\langle x(t;\Psi)\rangle_{as}$ of the system to the periodic modulation is a periodic function of time, i.e.,

$$\langle x(t;\Psi)\rangle_{as} = \int_0^\infty xP_{as}(x,t;\Psi)\mathrm{d}x = \sum_{n=-\infty}^{\infty} |M_n|\exp\left[in(\Omega t + \varphi_n + \Psi)\right]. \tag{2.9}$$

We can also understand our optical system as a sort of noisy nonlinear filter. The input signal is represented by the modulation of the incident light amplitude, while the output signal is given by the response $\langle x(t;\Psi)\rangle_{as}$. The transfer from the input to the output is controlled by the properties of the optical system *and by the noise*. Within this notation, the amplification of the signal is given by [3]

$$\eta_1 = 4\frac{|M_1|^2}{A^2}, \tag{2.10}$$

while higher harmonics in the response of the system are generated with the strength

$$\eta_n = 4\frac{|M_n|^2}{A^2}. \tag{2.11}$$

In the following we shall investigate and physically interpret the amplitudes (i.e., the strengths $\{\eta_n\}$) and the phases $\{\varphi_n\}$ of the complex-valued expansion coefficients $\{M_n\}$ in (2.9).

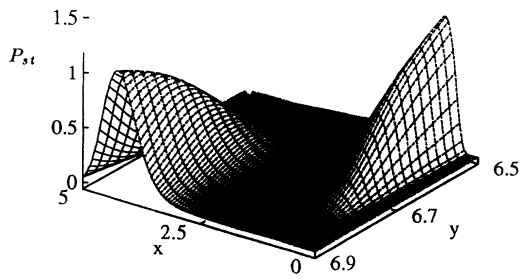

FIG. 3. The stationary probability distribution P_{st} of the undriven system ($A = 0$) [i.e., $y(t) = y_0$] is shown for the noise strength $D = 1$ and $c = 6$.

III. AMPLIFICATION OF THE OPTICAL SIGNAL

Due to the complex Fokker-Planck equation with multiplicative noise and the singular structure in the generalized potential $\Phi(x)$ we present in greater detail the reasoning underlying our numerical approach in the Appendix. In the following we present our numerical results together with analytical results based on the linear response theory [3,15]. The numerical study is based on a matrix-continued fraction solution of (2.6).

The amplification of the periodic input signal is measured by η_1; cf. (2.10) [3]. For the further discussion, we distinguish between the "symmetric" and the "asymmetric" case. In the symmetric case, the undriven stationary probability distribution $P_{st}(x)$ exhibits two peaks of equal weight in the zero-noise limit $D \to 0$ [i.e., the generalized potential Φ in (2.8b) possesses equal minima at the two metastable states]. In the asymmetric case $P_{st}(x)$ becomes unimodal in this limit $D \to 0$. For the numerical results presented below, we have always adopted an optical bistable situation with $c = 6$. This choice of the constant c implies for the symmetric case an input amplitude $y_0 = 6.72584...$.

A. The symmetric case

In Fig. 4(a), η_1 is depicted as a function of the noise strength D for various values of the modulation frequency Ω. The dotted lines show the results obtained within linear response theory, detailed in Sec. III C. The solid lines correspond to the numerical results which we have obtained by using the numerical procedure described in the Appendix.

The results look very much like those of a symmetric quartic double well potential [3]. For weak noise, the amplification of the signal increases with increasing noise strength, and reaches a maximum. This phenomenon is termed "stochastic resonance." The vertically dashed lines are an estimation for the position of the peaks obtained by matching timescales: without driving the system undergoes noise-induced jumps from one stable state to the other, characterized by the mean first passage times $T_{lu}(D)$ (from the lower to the upper stable state) and $T_{ul}(D)$ (reverse). In order that the transmitted intensity responds optimally to the periodic signal, which tilts the potential alternately to the left and right, it has to jump twice in one period of the signal, i.e., $T_{ul} + T_{lu} = T_s := \frac{2\pi}{\Omega}$ (a more precise transcendental equation for the peak position has been obtained recently in Ref. [4]). As expected from the arguments above, the location of maximal amplification as a function of noise

intensity D shifts to smaller values when the period of driving becomes larger.

B. The asymmetric case

As an example for an asymmetric case we have chosen $y_0 = 6.8$. In Fig. 4(b), $\eta_1(D)$ is shown for the same external driving frequencies as in Fig. 4(a). Here, the amplification approaches for decreasing driving frequencies Ω a limit curve, where the maximum is located at a finite, frequency-independent value of the noise strength. The matching of time scales used above to locate the position of the peak does not apply in the asymmetric case. This behavior can be explained as follows: the response of a noisy bistable system to periodic forcing is made up of both noise-assisted hopping between the potential wells and the relaxation dynamics within the wells. These two physical processes assume different weighting factors. The weight of the response due to hopping is for weak noise ($D \ll 1$) proportional to the Arrhenius factor $\exp\left(-\frac{\Delta\Phi}{D}\right)$, where $\Delta\Phi$ is the potential difference of the two metastable states. With $\Delta\Phi \neq 0$, this factor exponentially suppresses the amplification η_1 at weak noise; note also Sec. 6.3 in Ref. [15], Eqs. (6.3.25), (6.3.46), and (6.3.63) therein. Nevertheless, the drastically reduced amplification η_1—as compared to the symmetric case—still is of bell-shaped form, with the peak location shifted to higher noise intensities. It should be stressed, however, that the occurrence of the peak itself is still due to the hopping mechanism, see below (3.19). This very fact becomes evident if we describe the amplification within the approximation of linear response, being discussed in the following section.

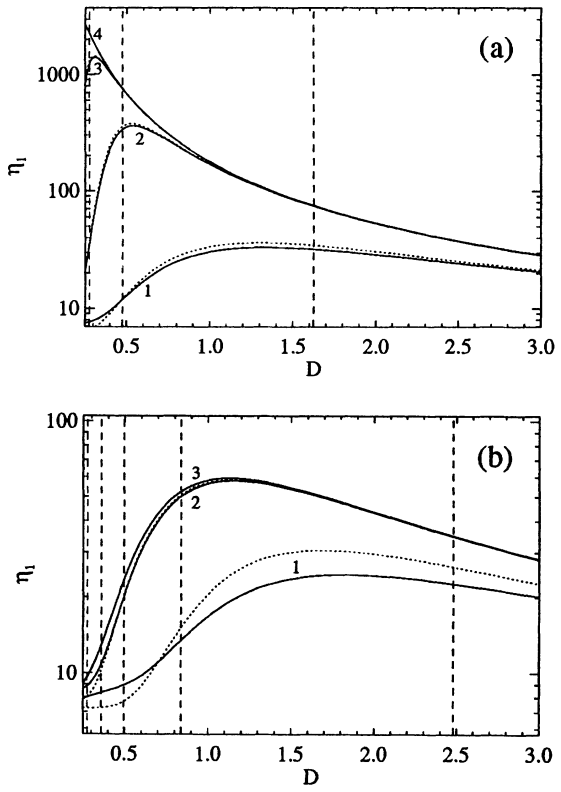

FIG. 4. The numerical results for the amplification η_1 are shown by the solid lines for the "symmetric case" $y_0 = 6.72584$ in (a) and the "asymmetric case" $y_0 = 6.8$ in (b) at $c = 6$ and $A = 10^{-4}$. Different lines labeled by "n" correspond to the external frequency $\Omega = 10^{-n}$. In (b), the curves for $\Omega < 10^{-3}$ are not distinguishable from the curve for $\Omega = 10^{-3}$. The dotted lines correspond to results within linear response approximation. They can only be distinguished from the numerical results for frequencies larger than about 10^{-2}. The vertical dashed lines indicate the position D_e of the maxima determined by the argument of matching time scales discussed in Sec. III A. In doing so, the mean first passage times $\{T_{ul}, T_{lu}\}$ have been numerically evaluated from the corresponding exact quadrature expression [14]. From right to left, these lines correspond to the values D_e at the driving frequency $\Omega = 10^{-1}, 10^{-2}, 10^{-3}, \ldots$, respectively, both in (a) and (b).

C. Linear response theory

For small amplitudes A we expand the full solution $P_{as}(x,t;\Psi)$ in a power series with respect to A, i.e.,

$$P_{as}(x,t;\Psi) = P_{st}(x) + A\,p(x,t;\Psi) + O(A^2). \tag{3.1}$$

The long-time response of the system to periodic forcing is given by

$$\Delta x(t;\Psi) := \langle x(t;\Psi)\rangle_{as} - \int_0^\infty x P_{st}(x)\mathrm{d}x$$

$$= \int_{-\infty}^{\infty} R(t-t')A\cos(\Omega t' + \Psi)\mathrm{d}t'. \tag{3.2}$$

Here, $R(t)$ denotes the response function

$$R(t) = \begin{cases} -\int x e^{L_{FP}(x)t}\frac{\partial}{\partial x}P_{st}(x)\mathrm{d}x, & \text{if } t \geq 0, \\ 0, & \text{if } t < 0, \end{cases} \tag{3.3}$$

where $L_{FP}(x)$ is the Fokker-Planck operator of the undriven system

$$L_{FP}(x) = -\frac{\partial}{\partial x}D^{(1)}(x) + \frac{\partial^2}{\partial x^2}D^{(2)}(x), \tag{3.4}$$

with $D^{(1)}(x)$ and $D^{(2)}(x)$ defined in (2.6b) and (2.6c). We can express the response function $R(t)$ in terms of a *generalized fluctuation-dissipation theorem* [15] by setting

$$R(t) = \frac{\mathrm{d}}{\mathrm{d}t}K_{xh}(t), \tag{3.5}$$

where

$$K_{xh}(t) := \langle x(t)h[x(0)]\rangle - \langle x\rangle_{st}\langle h(x)\rangle_{st}. \tag{3.6}$$

To determine the corresponding function $h(x)$, we use the formal solution of the correlation function [14]

$$K_{xh}(t) = \int x e^{L_{FP}(x)t}h(x)P_{st}(x)\mathrm{d}x. \tag{3.7}$$

Taking the derivative with respect to time, and using

$$D^{(1)}(x)P_{st}(x) = \frac{\partial}{\partial x}\left[D^{(2)}(x)P_{st}(x)\right], \tag{3.8}$$

we arrive at

$$\frac{\mathrm{d}}{\mathrm{d}t}K_{xh}(t) = \int x e^{L_{FP}t}\left\{\frac{\partial h}{\partial x}\frac{\partial[D^{(2)}(x)P_{st}(x)]}{\partial x} + \frac{\partial^2 h}{\partial x^2}\left[D^{(2)}(x)P_{st}(x)\right]\right\}\mathrm{d}x. \tag{3.9}$$

On the other hand Eq. (3.3) can be written as

$$\begin{aligned} R(t) &= -\int x e^{L_{FP}t}\frac{\partial}{\partial x}\left[\frac{1}{D^{(2)}(x)}D^{(2)}(x)P_{st}(x)\right]\mathrm{d}x \\ &= \int x e^{L_{FP}t}\left\{-\frac{1}{D^{(2)}(x)}\frac{\partial\left[D^{(2)}(x)P_{st}(x)\right]}{\partial x} + \frac{1}{\left[D^{(2)}(x)\right]^2}\frac{\partial D^{(2)}(x)}{\partial x}\left[D^{(2)}(x)P_{st}(x)\right]\right\}\mathrm{d}x. \end{aligned} \tag{3.10}$$

Upon comparing Eq. (3.9) with (3.10) the result then yields for the corresponding fluctuation in (3.5)

$$\begin{aligned} h(x) &= \int^x \frac{1}{D^{(2)}(x')}\mathrm{d}x' \\ &= \frac{1}{D}\left(-\frac{1}{x} + 2x + \frac{1}{3}x^3\right). \end{aligned} \tag{3.11}$$

$K_{xh}(t)$ can be approximated by a sum of three exponentials with the typical time scales of the system λ_T and $\lambda_{1,2}$—stemming from hopping (λ_T) between the potential wells and local motion ($\lambda_{1,2}$) within the wells, respectively, i.e.,

$$K_{xh}(t) \approx \sum_{m=1,2,T} g_m e^{-\lambda_m t}. \tag{3.12}$$

These time scales are given explicitly by [5,15]

$$\lambda_T = \left(\frac{1}{T_{lu}} + \frac{1}{T_{ul}}\right), \tag{3.13a}$$

$$\lambda_{1,2} = \left.\frac{\partial^2 V(x)}{\partial x^2}\right|_{x=x_l,x_u}. \tag{3.13b}$$

The times T_{lu} and T_{ul} denote the mean first passage times of the unperturbed system from the lower-intensity to the upper-intensity state, and vice versa, respectively, while the positions x_l and x_u denote the minima of the potential $V(x)$.

The amplification η_1 and the phase shift φ_1 follow from the leading Fourier-coefficient of $\Delta x(t;\Psi)$, Eqs. (3.2) and (2.9)–(2.11). Using the results of linear response (3.2), (3.5), and (3.12) we have

$$\Delta x(t;\Psi) = -\frac{A}{2}\sum_{m=1,2,T}\lambda_m g_m \times\left[\frac{e^{i(\Omega t+\Psi)}}{\lambda_m + i\Omega} + \frac{e^{-i(\Omega t+\Psi)}}{\lambda_m - i\Omega}\right]. \tag{3.14}$$

Thus the first Fourier-amplitude M_1 is given from (3.14) within linear response by

$$M_1 = -\frac{A}{2}\sum_{m=1,2,T}\frac{\lambda_m g_m e^{i\Psi}}{\lambda_m + i\Omega}. \tag{3.15}$$

The weights g_m are determined by matching the approximated correlation function (3.12) at $t = 0$ to the exact initial value and the first two initial derivatives, i.e.,

$$K_{x,h}(0) = \sum_{m=1,2,T} g_m = \langle xh(x)\rangle_{st} - \langle x\rangle_{st}\langle h(x)\rangle_{st} \tag{3.16a}$$

and

$$\left.\frac{\mathrm{d}}{\mathrm{d}t}K_{x,h}(t)\right|_{t=0} = -\sum_{m=1,2,T}\lambda_m g_m = \left\langle D^{(1)}(x)h(x)\right\rangle_{st}, \tag{3.16b}$$

$$\begin{aligned} \left.\frac{\mathrm{d}^2}{\mathrm{d}t^2}K_{x,h}(t)\right|_{t=0} &= \sum_{m=1,2,T}\lambda_m^2 g_m \\ &= \left\langle\left(D^{(1)}(x)\frac{\partial D^{(1)}(x)}{\partial x} + D^{(2)}(x)\frac{\partial^2 D^{(1)}(x)}{\partial x^2}\right)h(x)\right\rangle_{st}. \end{aligned} \tag{3.16c}$$

By simplifying the expressions for the mean values in Eqs. (3.16b) and (3.16c) by use of the property

$$\begin{aligned} \left\langle L_{FP}^{+}(x)p(x)\right\rangle_{st} &= \left\langle D^{(1)}(x)\frac{\partial p(x)}{\partial x}\right\rangle_{st} \\ &\quad + \left\langle D^{(2)}(x)\frac{\partial^2 p(x)}{\partial x^2}\right\rangle_{st} = 0, \end{aligned} \tag{3.17}$$

where

$$L_{FP}^{+}(x) = D^{(1)}(x)\frac{\partial}{\partial x} + D^{(2)}(x)\frac{\partial^2}{\partial x^2} \tag{3.18}$$

is the Hermitian adjoint operator of $L_{FP}(x)$, we finally obtain

$$\left.\frac{\mathrm{d}}{\mathrm{d}t}K_{x,h}(t)\right|_{t=0} = 1, \tag{3.19a}$$

$$\left.\frac{\mathrm{d}^2}{\mathrm{d}t^2}K_{x,h}(t)\right|_{t=0} = \left\langle\frac{\partial D^{(1)}(x)}{\partial x}\right\rangle_{st}. \tag{3.19b}$$

The weights $\{g_m\}$ are obtained from the set of equations (3.16a), (3.19a), and (3.19b).

The results of the linear response approximation are shown in Figs. 4(a) and 4(b) by dotted lines for the symmetric and the asymmetric case, respectively. In both cases we find excellent agreement for not too large frequencies Ω.

To analyze whether the maximum in η_1 actually stems from the hopping process, we *neglected* in the linear response approximation the eigenvalues λ_1 and λ_2, characterizing the intrawell motion, and retained only the eigenvalue λ_T. For both, the symmetric as well as for the asymmetric situation, we still find excellent agreement around the maximum of η_1 and for larger values of the noise strength. The behavior for $D \to 0$, however, is not reproduced correctly. Here, the response due to the motion within the wells becomes dominating. This

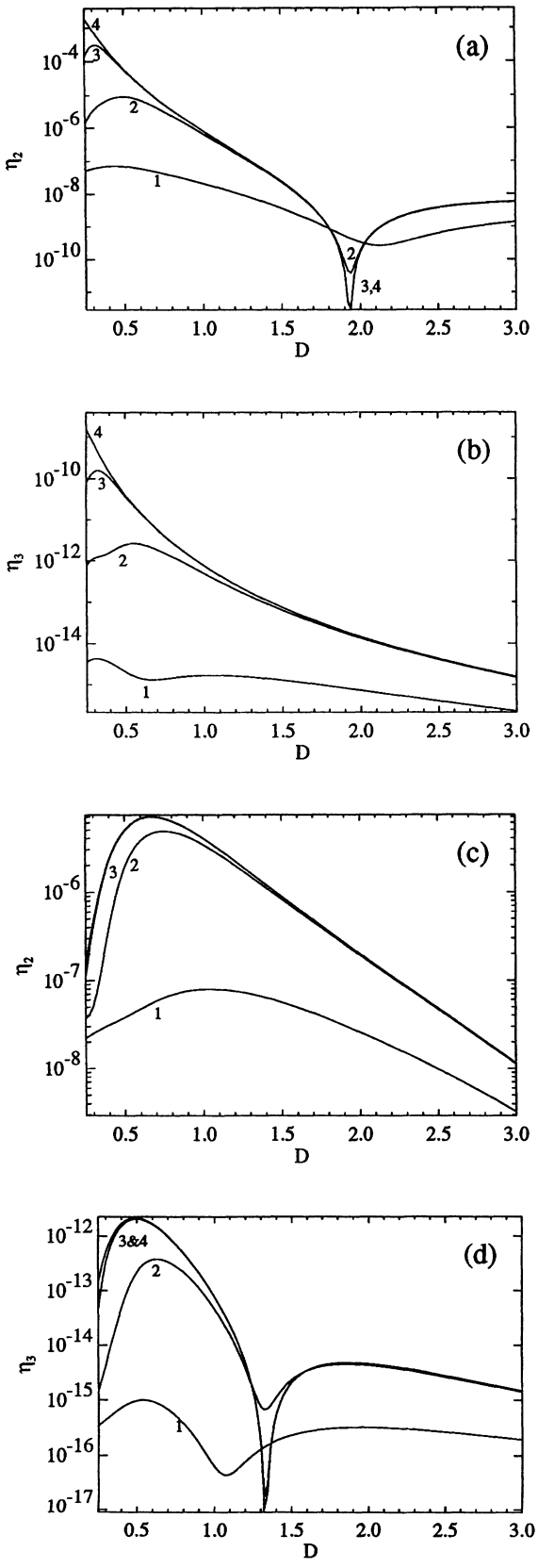

FIG. 5. The generation strengths for higher harmonics are shown for the symmetric (a),(b) and asymmetric case (c),(d) at $c = 6$ and $A = 10^{-4}$. The values of the driving frequency are the same as in Fig. 4, i.e., line "n" corresponds to $\Omega = 10^{-n}$.

emphasizes the fact that in the symmetric *as well as in the asymmetric case* stochastic resonance is due to the interplay of hopping between wells and the deterministic modulation, i.e., the maximal amplification characteristic for stochastic resonance is practically not affected by the motion within the potential wells [16,17].

IV. GENERATION OF HIGHER HARMONICS

Most of the studies in stochastic resonance are restricted to the discussion of the amplification η_1, or the corresponding signal-to-noise ratio [1–7]. In this section, we study for the first time to what extent the generation of higher harmonics generated by a nonlinear system exhibiting stochastic resonance is affected by the noise. In Fig. 5 we have plotted the generation strengths η_n for the second and third harmonic at the same values of the signal frequency Ω used in Fig. 4 for the signal amplification η_1.

In the symmetric case [see Figs. 5(a) and 5(b)] the generation strengths η_2 and η_3 exhibit a typical stochastic resonance curve (at very small frequencies Ω those parts of the curves which show a steep increase with increasing noise strength are not shown). More surprisingly, a peculiar resonance-absorption-like dip, which we term *noise-induced resonances (NIR)*, shows up in the second harmonic, when the signal frequency decreases. However, the third harmonic does not exhibit such NIR in the symmetric case.

In the asymmetric case [Figs. 5(c) and 5(d)], the generation strengths for the higher harmonics approach limit curves for small, decreasing frequencies Ω. In contrast to the symmetric case, we now observe NIR in the *third harmonic*.

To confirm the occurrence of noise-induced resonances, we have compared the numerical results with those obtained from the adiabatic approximation [18]. The result is shown in Fig. 6: the solid line corresponds to the numerical result, whereas the dotted line depicts the adiabatic approximation. For the adiabatic approximation to be valid in a large range of noise intensities we

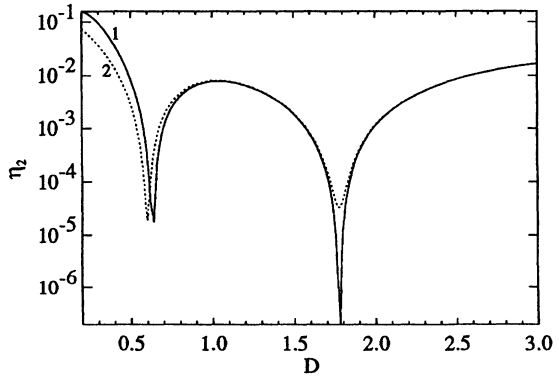

FIG. 6. In the symmetric case, the numerical result for the generation strength of the second harmonic η_2 (line 1, solid) is compared with the adiabatic approximation (line 2, dotted) at $c = 6$, $A = 0.31623$, and $\Omega = 10^{-6}$.

have chosen a driving frequency $\Omega = 10^{-6}$. For example, if we focus on η_2, Fig. 6 demonstrates that more than one dip can occur in the dependence of generation strength versus noise intensity. At present times, we—unfortunately—have no simple physical explanation for these novel phenomena.

The phenomenon of noise-induced resonances together with the corresponding phase jumps actually occur under very general circumstances. In Ref. [9] noise-induced resonances have been found in asymmetric bistable as well as in asymmetric *monostable* nonlinear systems. It has been analyzed analytically for a bistable system by using an asymmetric two-state approach in [9]. Noise-induced resonances seem to be universal for asymmetric nonlinear noisy filters, but still need to be investigated experimentally.

V. PHASE SHIFTS

Upon inspecting (2.9) we note that the asymptotic mean value involves complex-valued Fourier coefficients $\{M_n\}$. It is of interest to investigate the behavior of the corresponding phases $\{\varphi_n\}$ of (2.9)—which induce a characteristic *lag* of the deterministic phase $(\Omega t + \Psi)$—as a function of the parameters characterizing the stochastic resonance.

In Fig. 7(a), the phase lag of the fundamental har-

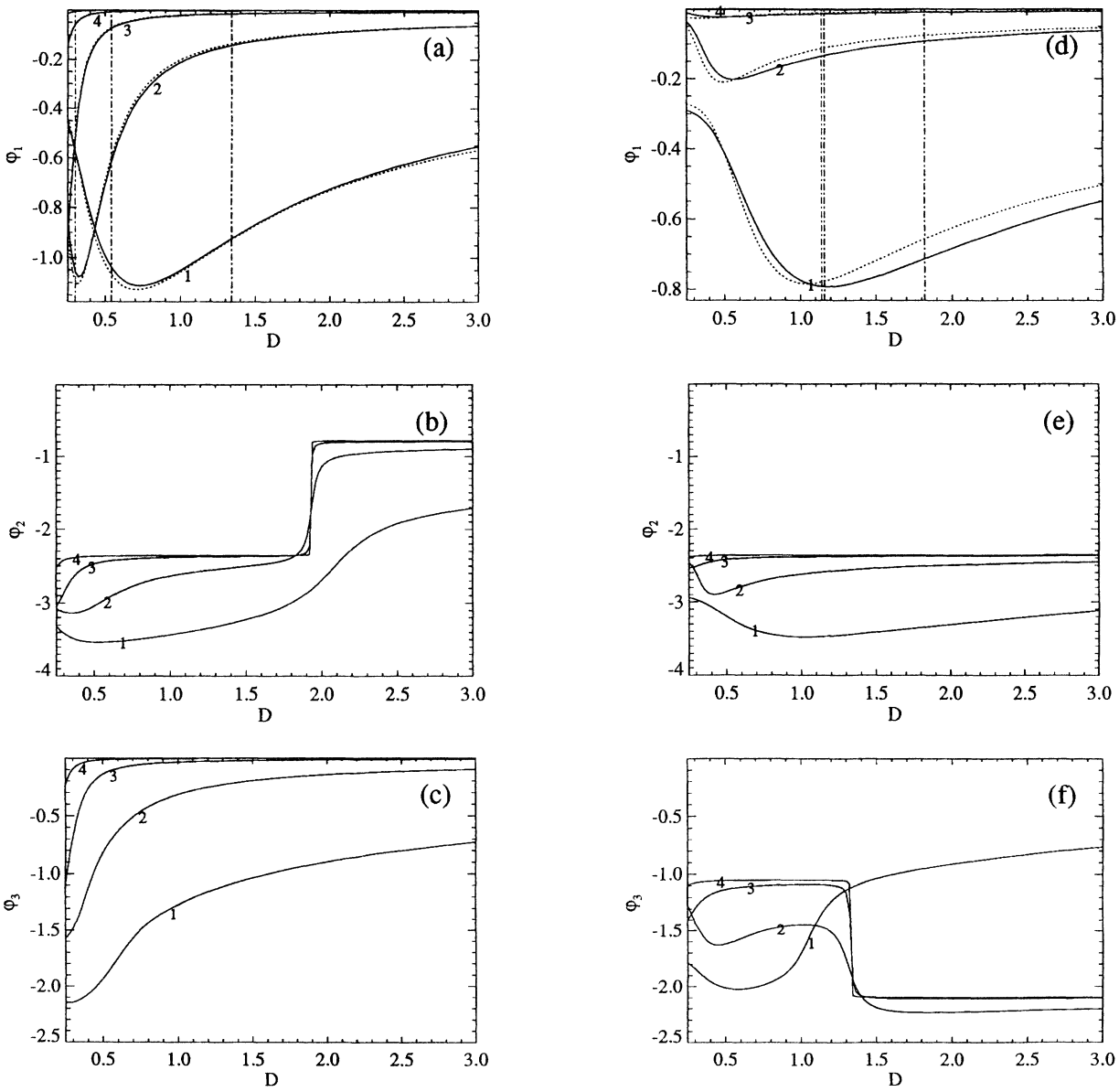

FIG. 7. The phase shifts for the symmetric (a)–(c) and asymmetric (d)–(e) case are shown at $c = 6$, $A = 10^{-4}$. The lines labeled with "n" correspond to values of the driving frequency $\Omega = 10^{-n}$. In (d), line 4 ($\Omega = 10^{-4}$) coincides with the axes $\varphi_1 = 0$. The dotted lines in (a) and (d) show the results of the linear response approximation. The vertical dashed-dotted lines in (a) and (d) represent the positions of the corresponding maxima in η_1, cf. Fig. 4. From right to left these vertical lines correspond to the curves labeled by "n"=1,2,3.

monic φ_1 is shown as a function of the noise intensity for the symmetric case. In addition, the positions of the maxima of the numerically calculated amplifications η_1 are depicted by vertical dashed-dotted lines. With weak noise, φ_1 decreases for increasing noise strength, reaches a minimum, and increases again with further increasing noise intensity. Although this behavior has intriguing similarities with stochastic resonance, *the minimum of the phase lag is actually not related to stochastic resonance.* The minimum in the phase shift marks the transition from a hopping-motion dominated behavior to an intrawell motion dominated dynamics [17].

In Fig. 7(d), the phase lag φ_1 is shown in the asymmetric case and the vertical dashed-dotted lines again represent the positions of the maxima of η_1. Here, the phase lag φ_1 shows a minimum similar as in the symmetric case. By decreasing the driving frequency further, however, the minimum of the phase moves towards smaller values of the noise strength. In contrast to the amplification η_1 [cf. Fig. 4(b)], the phase φ_1, as a function of the noise D, does not approach a limit curve as $\Omega \to 0$. This discrepancy between the minimum of the phase and the maximum of the amplification emphasizes their different physical origin.

In Figs. 7(b) and 7(c), the phases are shown for the second and third harmonic in the symmetric case. Most significantly, the phase of the second harmonic φ_2 as a function of the noise strength D assumes for decreasing driving frequency $\Omega \to 0$ a step function with the discontinuity occurring *exactly at that value* of the noise strength where we observed NIR. In Figs. 7(e) and 7(f), the phases of the higher harmonics are shown as a function of the noise in the asymmetric case. Similarly as in the symmetric case, we observe phase jumps at those values of the noise strength, where we found NIR.

In both cases the phase jumps $\Delta\varphi_n$ approach the value of (π/n), n=2,3, for decreasing signal frequencies. This fact also holds true for $n = 4$ and $n = 5$ (not shown in Fig. 7). All of these characteristic behaviors emerge also within the regime of validity of the adiabatic approximation [3].

VI. CONCLUSIONS

We presented a detailed study of the phenomenon of stochastic resonance in a model for absorptive optical bistability. In contrast to the case with symmetric bistability discussed in previous works [1–5] we investigated stochastic resonance in a system which possesses both, symmetric and asymmetric bistability. In doing so, we found a significantly different behavior of the signal amplification as compared to the symmetric case: in the weak noise limit the signal amplification η_1 is *exponentially suppressed* in the asymmetric case, yielding a peak position being not in accord with the reasoning involving the matching of time scales for external driving and over-barrier hopping. We further confirmed that for symmetric as well as for asymmetric systems the phenomenon of stochastic resonance is not phase sensitive, i.e., the phase does not show any characteristic effect at the value of the noise strength where we observe stochastic resonance. Moreover, we discovered a novel noise-induced resonance mechanism. The generation strengths of some higher harmonics η_n, n=2,3, exhibit a *resonance-absorption-like* dip at certain values of the noise strength. This characteristic dip becomes very sharp as the signal frequency Ω approaches zero. Thus far, the physics of these dips could be explained within the adiabatic approximation only; cf. Fig. 6. This resonance absorption is—in contrast to stochastic resonance—phase sensitive: we observe characteristic phase jumps of values (π/n) precisely at those parameter values where NIR occurs.

These novel phenomena (i.e., "dips" and "jumps") cannot be explained on a deterministic level, which implies a zero noise intensity ($D = 0$). At present, these features still await a simple physical intuitive explanation. We hope that this work will stimulate future research which hopefully will disentangle in greater detail these complex novel features.

ACKNOWLEDGMENTS

This work has been supported by the Volkswagen Foundation, Az. I/65 037-1, "Resonanzaktivierung" (P.H.), and the Deutsche Forschungsgemeinschaft (P.J.).

APPENDIX: NUMERICAL SOLUTION

In order to apply the method of matrix continued fraction for the solution of the Fokker-Planck equation (2.6), we use instead of the probability density $P(x,t;\Psi)$ the function

$$\rho(x,t;\Psi) := \frac{P(x,t;\Psi)}{x(1+x^2)^3}. \tag{A1}$$

This function satisfies the equation of motion

$$(1+x^2)^3 x \frac{\partial}{\partial t}\rho(x,t;\Psi) = \hat{L}_0\rho(x,t;\Psi) + \hat{L}_1\rho(x,t;\Psi)\cos(\Omega t+\Psi) \tag{A2}$$

with the operators given by

$$\hat{L}_0 = -\frac{\partial}{\partial x}\left[(1+x^2)^3 x(y_0-x) - 2c(1+x^2)^2x^2 + Dx^2(1-x^2)\right] + D\frac{\partial^2}{\partial x^2}x^3(1+x^2), \tag{A3a}$$

$$\hat{L}_1 = -A\frac{\partial}{\partial x}\left[(1+x^2)^3 x\right]. \tag{A3b}$$

Note that the introduction of the auxiliary function $\rho(x,t;\Psi)$ leads to the property that—in contrast to (2.6)—the operators $\hat{L}_0$ and $\hat{L}_1$ contain no rational functions.

The asymptotic probability density $P_{as}(x,t;\Psi)$, and thus also the corresponding asymptotic function $\rho_{as}(x,t;\Psi)$, can be expanded into a Fourier series with respect to time and into the complete set of Laguerre polynomials with respect to x, i.e.,

$$\rho_{as}(x,t;\Psi) = \frac{1}{N}\sum_{n=-\infty}^{\infty}\sum_{p=0}^{\infty} c_n^p(\alpha,\lambda)\exp\left[in(\Omega t+\Psi)\right] t_p^{(\alpha)}(\lambda x), \tag{A4}$$

with complex-valued coefficients $c_n^p(\alpha,\lambda)$. The parameter α in (A4) always obeys $\alpha > -1$ (see below). The scaling parameter λ is real valued and positive, but otherwise arbitrary. The parameters α and λ are chosen in order to optimize the convergence of the numerical procedure. The constant N is used to normalize the asymptotic probability density according to

$$\int_0^\infty P_{as}(x,t;\Psi)\mathrm{d}x = 1. \tag{A5}$$

The Laguerre functions $t_p^{(\alpha)}(\lambda x)$ are defined by the Laguerre polynomials $L_p^{(\alpha)}(\lambda x)$ [13] as

$$t_p^{(\alpha)}(\lambda x) := e^{-\lambda x}(\lambda x)^\alpha L_p^{(\alpha)}(\lambda x). \tag{A6}$$

They meet the orthogonality relation

$$\int_0^\infty L_q^{(\alpha)}(\lambda x) t_p^{(\alpha)}(\lambda x)\mathrm{d}x = \delta_{q,p}\frac{\Gamma(\alpha+p+1)}{p!\lambda} =: \Delta_{qp}^{\alpha\lambda}. \tag{A7}$$

Further, they obey the recurrence relations

$$x t_p^{(\alpha)}(\lambda x) = \frac{1}{\lambda}\Big[-(p+1)t_{p+1}^{(\alpha)}(\lambda x) + (2p+\alpha+1)t_p^{(\alpha)}(\lambda x) - (p+\alpha)t_{p-1}^{(\alpha)}(\lambda x)\Big], \tag{A8a}$$

and

$$x\frac{\partial}{\partial x}t_p^{(\alpha)}(\lambda x) = (p+1)\left[t_{p+1}^{(\alpha)}(\lambda x) - t_p^{(\alpha)}(\lambda x)\right]. \tag{A8b}$$

To abbreviate products of the form $x^n t_p^{(\alpha)}(\lambda x)$ we introduce the quantities $\{{}^p m_j^n\}$, defined by

$$x^n t_p^{(\alpha)}(\lambda x) =: \sum_{j=-n}^{n} {}^p m_j^n\, t_{p+j}^{(\alpha)}(\lambda x). \tag{A9}$$

The numbers $\{{}^p m_j^n\}$ follow from (A8a) by iteration, i.e.,

$${}^p m_0^0 = 1, \tag{A10a}$$

$${}^p m_j^n = 0 \text{ for all } |j| > n, \tag{A10b}$$

$${}^p m_j^n = \frac{1}{\lambda}\left[\Upsilon_{0,j}\,{}^p m_j^{n-1}(2p+2j+1) - \Upsilon_{1,j}\,{}^p m_{j-1}^{n-1}(p+j) - \Upsilon_{2,j}\,{}^p m_{j+1}^{n-1}(p+j+1+\alpha)\right], \tag{A10c}$$

where

$$\Upsilon_{0,j} = \begin{cases} 1, \text{if } -n+1 \le j \le n-1, \\ 0, \text{ otherwise,} \end{cases}$$

$$\Upsilon_{1,j} = \begin{cases} 1, \text{if } -n+2 \le j \le n, \\ 0, \text{ otherwise,} \end{cases}$$

$$\Upsilon_{2,j} = \begin{cases} 1, \text{if } -n \le j \le n-2, \\ 0, \text{ otherwise.} \end{cases} \tag{A10d}$$

Inserting (A4) into the equation of motion (A2) and using the orthogonality and recursion properties of the Laguerre functions, we obtain for the vectors $\mathbf{c}_n := (c_n^0, c_n^1, \ldots)^T$ the vector recurrence relation

$$\mathbf{Q}_n^- \mathbf{c}_{n-1} + \mathbf{Q}_n \mathbf{c}_n + \mathbf{Q}_n^+ \mathbf{c}_{n+1} = \mathbf{0}. \tag{A11}$$

The matrices $\mathbf{Q}_n^- = \mathbf{Q}_n^+$ are real-valued, while the matrix $\mathbf{Q}_n$ has the complex-valued elements

$$(\mathbf{Q}_n)_{qp} =: Q_0^{qp} - in\Omega Q_1^{qp}. \tag{A12a}$$

The real-valued elements of all matrices are given by

$$(\mathbf{Q}_n^+)_{qp} = -\frac{A}{2}\sum_{j=-6}^{6}\Big\{\Delta_{q\,p+j}^{\alpha\lambda}\left[-{}^p m_j^0 p + {}^p m_j^2(6-3p) + {}^p m_j^4(12-3p) + {}^p m_j^6(6-p)\right] + \Delta_{q\,p+j+1}^{\alpha\lambda}(p+1)\left[-{}^{p+1} m_j^0 p + {}^{p+1} m_j^2 3 + {}^{p+1} m_j^4 3 + {}^{p+1} m_j^6\right]\Big\}, \tag{A12b}$$

$$Q_1^{qp} = \sum_{j=-7}^{7}\Delta_{q\,p+j}^{\alpha\lambda}\left[{}^p m_j^1 + {}^p m_j^3 3 + {}^p m_j^5 3 + {}^p m_j^7\right], \tag{A12c}$$

$$\begin{aligned} Q_0^{qp} = \sum_{j=-7}^{7}\Big\{&\Delta_{q\,p+j}^{\alpha\lambda}\left[{}^p m_j^0 y_0 p + {}^p m_j^1(1-p)(1+2c+D(1-p)) + {}^p m_j^2 3y_0(p-2)\right. \\ &+ {}^p m_j^3\left[(1-p)(3+4c+(7-p)D) + 6 + 8c + 8D\right] + {}^p m_j^4 3y_0(p-4) \\ &\left. + {}^p m_j^5(15+10c-p(3+2c)) + {}^p m_j^6 y_0(p-6) + {}^p m_j^7(7-p)\right] \\ &+ \Delta_{q\,p+j+1}^{\alpha\lambda}(p+1)\left[-{}^{p+1} m_j^0 y_0 + {}^{p+1} m_j^1(1+2c+D-2pD)\right. \\ &- {}^{p+1} m_j^2 3y_0 + {}^{p+1} m_j^3(3+4c+7D-2pD) \\ &\left. - {}^{p+1} m_j^4 3y_0 + {}^{p+1} m_j^5(3+2c) - {}^{p+1} m_j^6 y_0 + {}^{p+1} m_j^7\right] \\ &+ \Delta_{q\,p+j+2}^{\alpha\lambda}(p^2+3p+2)D\left[{}^{p+2} m_j^1 + {}^{p+2} m_j^3\right]\Big\}. \end{aligned} \tag{A12d}$$

In a similar way we find from the condition for the normalization (A5)

$$
\begin{aligned}
N &= \sum_{n=-\infty}^{\infty} \exp\left[in(\Omega t+\Psi)\right] \\
&\quad \times \sum_{p=0}^{\infty} c_n^p \int_0^{\infty} x(1+x^2)^3 t_p^{(\alpha)}(\lambda x)\mathrm{d}x \\
&= \sum_{n=-\infty}^{\infty} \exp\left[in(\Omega t+\Psi)\right] \\
&\quad \times \sum_{p=0}^{7} c_n^p \left({}^0m_p^1 + 3^0m_p^3 + 3^0m_p^5 + {}^0m_p^7\right) \Delta_{pp}^{\alpha\lambda} \\
&= \sum_{p=0}^{7} c_0^p \left({}^0m_p^1 + 3^0m_p^3 + 3^0m_p^5 + {}^0m_p^7\right) \Delta_{pp}^{\alpha\lambda}. \qquad \text{(A13)}
\end{aligned}
$$

The tridiagonal vector recurrence relation Eq. (A11) can be solved for the coefficients $\{\mathbf{c}_n\}$ by using the method of matrix continued fractions [14]. The Fourier series of $\langle x(t;\Psi)\rangle_{as}$, which is the basis for the calculation of the amplification and the generation strengths of higher harmonics (2.10) and (2.11), is thus written in terms of the expansion coefficients $\{c_n^p\}$ as

$$
\langle x(t;\Psi)\rangle_{as} = \sum_{n=-\infty}^{\infty} M_n \exp\left[in(\Omega t+\Psi)\right], \qquad \text{(A14)}
$$

where

$$
M_n = \frac{1}{N}\sum_{p=0}^{\infty} c_n^p u_p \qquad \text{(A15)}
$$

and

$$
\begin{aligned}
u_p &\equiv \int_0^{\infty} x t_p^{(\alpha)}(\lambda x) x(1+x^2)^3 \mathrm{d}x \\
&= \Delta_{p\,p}^{\alpha\lambda}\left[{}^0m_p^2 + 3^0m_p^4 + 3^0m_p^6 + {}^0m_p^8\right]. \qquad \text{(A16)}
\end{aligned}
$$

The amplitudes $\{|M_n|\}$ and thus the amplification η_1 and higher order generation strengths $\{\eta_n\}$ follow from (A15), while the corresponding phases introduced in (2.9) are given by

$$
\varphi_n = \frac{1}{n}\arctan\left[\frac{\mathrm{Im}(M_n)}{\mathrm{Re}(M_n)}\right]. \qquad \text{(A17)}
$$

[1] R. Benzi, A. Sutera, and A. Vulpiani, J. Phys. A **14**, L453 (1981); C. Nicolis, Tellus **34**, 1 (1982); P. Jung and P. Hänggi, Europhys. Lett. **8**, 505 (1989); L. Gammaitoni, F. Marchesoni, E. Menichella-Saetti, and S. Santucci, Phys. Rev. Lett. **62**, 349 (1989); Phys. Rev. A **40**, 2114 (1989); R. Fox, *ibid.* **39**, 4148 (1989); A. Bulsara, E. W. Jacobs, T. Zhou, F. Moss, and L. Kiss, J. Theor. Biol. **152**, 531 (1991); Hu Gang, T. Ditzinger, C. Z. Ning, and H. Haken, Phys. Rev. Lett. **71**, 807 (1993); M. I. Dykman, R. Manella, P. V. E. McClintock, N. D. Stein, and N. G. Stocks, Phys. Rev. E **47**, 1624 (1993); see also the collection of papers in J. Stat. Phys. **70**, No. 1/2 (1993).

[2] B. McNamara, K. Wiesenfeld, and R. Roy, Phys. Rev. Lett. **60**, 2626 (1988); G. Vemuri and R. Roy, Phys. Rev. A **39**, 4668 (1989).

[3] P. Jung and P. Hänggi, Phys. Rev. A **44**, 8032 (1991).

[4] R. F. Fox and Y. N. Lu, Phys. Rev. E **48**, 3390 (1993).

[5] P. Jung, Phys. Rep. **234**, 175 (1993).

[6] S. Fauvet and F. Heslot, Phys. Lett. **97A**, 5 (1983).

[7] J. K. Douglass, L. Wilkens, E. Pantazelou, and F. Moss, Nature (London) **365**, 337 (1993).

[8] R. Landauer, J. Appl. Phys. **32**, 2209 (1962); R. F. Fox, Phys. Rep. **48C**, 179 (1978); P. Hänggi, Phys. Lett. **78A**, 304 (1980); P. Hänggi and P. Jung, IBM J. Res. Dev. **32**, 119 (1988); B. J. West and K. Lindenberg, in *Studies in Statistical Mechanics, Vol. XIII*, edited by J. L. Lebowitz (North-Holland, Amsterdam, 1988), Chap. 2; M. L. Spano, M. Wun-Fogle, and W. L. Ditto, Phys. Rev. A **46**, 5253 (1992).

[9] P. Jung and R. Bartussek, in *Fluctuations and Order: The New Synthesis*, edited by M. Millonas (Springer, New York, 1994).

[10] R. Bonifacio and L. A. Lugiato, Phys. Rev. A **18**, 1192 (1978).

[11] A. R. Bulsara, W. C. Schieve, and R. F. Gragg, Phys. Lett. **68A**, 294 (1978); P. Hänggi, A. R. Bulsara, and R. Janda, Phys. Rev. A **22**, 671 (1980).

[12] P. Jung and P. Hänggi, Europhys. Lett. **8**, 505 (1989).

[13] *Handbook of Mathematical Functions*, edited by M. Abramowitz and I. A. Stegun (Dover, New York, 1965).

[14] H. Risken, *The Fokker-Planck-Equation* (Springer, Berlin, 1984).

[15] P. Hänggi and H. Thomas, Phys. Rep. **88C**, 207 (1982), see Sec. 5.2 and Sec. 6.3.

[16] L. Gammaitoni, M. Martinelli, L. Pardi, and S. Santucci, Phys. Rev. Lett. **67**, 1799 (1991).

[17] P. Jung and P. Hänggi, Z. Phys. B **90**, 255 (1993).

[18] P. Jung, Z. Phys. B **76**, 521 (1989).

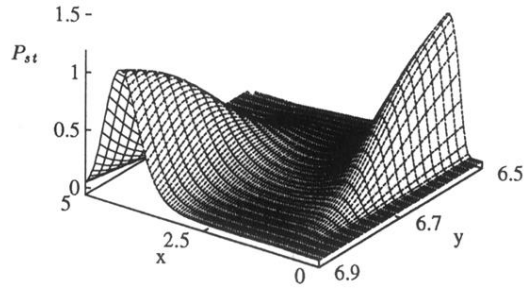

FIG. 3. The stationary probability distribution P_{st} of the undriven system ($A = 0$) [i.e., $y(t) = y_0$] is shown for the noise strength $D = 1$ and $c = 6$.